Nat Hazards (2016) 83:929–945
DOI 10.1007/s11069-016-2356-3

ORIGINAL PAPER

Study and numerical modeling of 1945 Makran tsunami due to a probable submarine landslide

Ehsan Rastgoftar[1] · Mohsen Soltanpour[2]

Received: 27 July 2015 / Accepted: 16 May 2016 / Published online: 28 May 2016

Abstract The Makran subduction zone (MSZ), located along the southern coasts of Iran and Pakistan, has experienced some deadly earthquakes and tsunamis, including the destructive 1945 Makran tsunami that led to more than 4000 fatalities. In spite of past studies on 1945 Makran tsunami, there are still unresolved problems, particularly on mismatches between the tsunami wave heights and arrival times with reported observations at different locations. The significant disagreement between the results of numerical models and existing data supports the existence of another mechanism involved during the generation of the tsunami. In the present study, a submarine landslide, triggered by the 1945 Earthquake, is studied as the major source of 1945 Makran tsunami. The simulation of seismic 1945 Tsunami, using high-resolution bathymetry data with a fine nested grid to increase the accuracy of modeled tsunami wave heights, confirms the large discrepancies between the reported tsunami waves and simulated values. Assuming the location and dimensions of a probable landslide, the GEOWAVE model, a combination of TOPICS and FUNWAVE models, is applied to model the non-seismic 1945 Tsunami. The simulated landslide tsunami demonstrates a fair agreement with the reported tsunami wave heights at different locations in Pakistan, Iran and India. The arrival times of tsunami waves at Pasni and Karachi in Pakistan can also be interpreted if the occurrence time of the probable submarine landslide is assumed with 3.5 h delay after the quake. The study highlights the potential danger of a non-seismic landslide tsunami in unconsolidated sediments at the

Ehsan Rastgoftar was Formerly Graduate Student, K.N. Toosi University of Technology, Tehran, Iran.

✉ Ehsan Rastgoftar
e.rastgoftar@inio.ac.ir

Mohsen Soltanpour
soltanpour@kntu.ac.ir

[1] National Institute for Oceanography and Atmospheric Science, No. 3, Etemad Zadeh St., Fatemi Ave., Tehran 14118-13389, Iran

[2] Department of Civil Engineering, K. N. Toosi University of Technology, No. 1364, Vali-Asr St., Tehran 19967-15433, Iran

MSZ and the necessity of the development of suitable countermeasures against other potential Makran tsunamis in future.

Keywords Tsunami simulation · Makran subduction zone (MSZ) · Submarine landslide · GEOWAVE model

1 Introduction

Tsunami waves can be generated by a rapid deformation in the seafloor topography, resulting from undersea landslides, volcanic eruptions or tectonic displacements. The recent destructive events of 2004 Indian Ocean Tsunami and 2011 Tohoku Earthquake Tsunami have proved the importance of the study and research on tsunamis. Although the majority of reported tsunamis have taken place in countries bordering the Pacific Ocean, 2004 Indian Ocean Tsunami caused widespread damages to eight countries and resulted in more than 225,000 fatalities, highlighting the necessity for studies to assess the risk of tsunamis in other parts of the world.

The Makran subduction zone (MSZ) and Sunda subduction zone are two tsunamigenic zones in the Indian Ocean (UNESCO/IOC 2009). The MSZ is located at the boundary of the Eurasian and Arabian plates in the northwestern part of the Indian Ocean (Fig. 1). It extends about 900 km from the Strait of Hormoz to the vicinity of Karachi in the southern coasts of Iran and Pakistan. The results of a recent research, carried out based on thermal modeling of the MSZ by Smith et al. (2013), have shown that past assumptions may have significantly underestimated the earthquake and tsunami hazard in the MSZ, that is

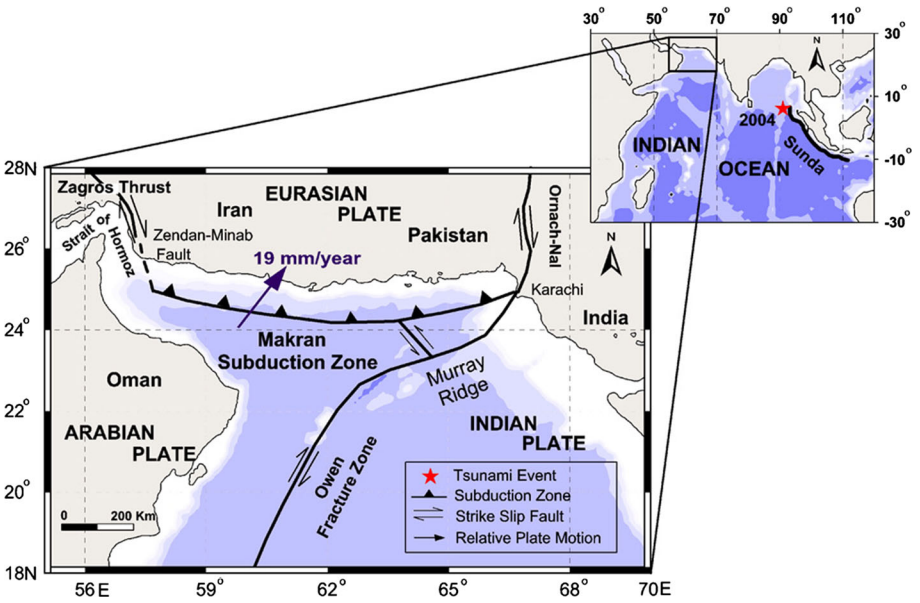

Fig. 1 Tectonic map of the MSZ at the northwestern part of Indian Ocean (Heidarzadeh et al. 2008)

potentially capable of producing major earthquakes, up to M_w 8.7–9.2. Although the seismic activity and potential for tsunami generation of MSZ is smaller than that of the Sunda subduction zone, it has experienced some deadly earthquakes and tsunamis. The oldest available record is the historical 326 BC Tsunami, which reportedly destroyed the Macedonian fleet of Alexander the Great when he was returning to Greece by a sea route (Lisitzin 1974). Past studies also reveal a number of other tsunamis in the North Indian Ocean (Murty and Bapat 1999) including the 1945 Makran tsunami, which is likely the most destructive tsunami in the Indian Ocean after the 2004 Indian Ocean Tsunami (Heidarzadeh et al. 2008).

In spite of the large number of past studies on the 1945 Makran tsunami in the MSZ (e.g., Rajendran et al. 2008; Heidarzadeh et al. 2009), some important problems are not yet resolved, particularly regarding mismatches of both tsunami wave heights and arrival times with observations at different locations. The occurrence of a secondary tsunami, generated by a submarine mudslide triggered by the earthquake, is one possible hypothesis for this event. However, no quantitative analysis of this scenario has yet been conducted, i.e., there are no estimates of exactly when and where this mudslide occurred.

In this study, for the first time, a submarine landslide after 1945 earthquake is presented as the possible major source of the 1945 tsunami, in order to explain the observations of tsunami wave heights and arrival times at different locations. In order to do so, the 1945 tsunami was first simulated based on the assumption of a seismic source using a fine localized nested grid to reduce the computational errors. The tsunami due to the landslide was then simulated by making some assumptions regarding its possible location and the dimensions of the slide. Besides the tsunami wave heights reported by past studies, the newly available data on inundation along the Iranian coast by Hamzeh et al. (2013) and Okal et al. (2015) was also employed for the verification of this scenario.

2 1945 Makran tsunami

In the early hours (about 3:00 a.m. at local time) of November 28, 1945 (21:56 UTC on 27 November), the Makran coast was shaken by a huge M_w 8.1 earthquake (Ambraseys and Melville 1982). The epicenter was located in the offshore of Pasni at 25.15°N and 63.48°E (Byrne et al. 1992). Although the number of fatalities due to the earthquake was <300, the subsequent tsunami increased the death toll to more than 4000 (Heck 1947). Maximum tsunami damage was reported in Pasni and Ormara, where at least three tsunami waves attacked the towns. The first wave, noticed shortly after the quake struck, did not come very far inland, while the other two followed about 90 and 120 min later and swept over the one-story houses at Pasni and Ormara, causing great damage, reaching heights of 5–10 m at the shore (Ambraseys and Melville 1982). While Pendse (1946) reported wave heights of about 12–15 m at Pasni, Berninghausen (1966) mentioned 12–15 m at both Pasni and Ormara.

Aside from Pasni and Ormara, tsunami waves also caused damage and casualties in some other neighboring coasts. Ambraseys and Melville (1982) reported that at Karachi, 360 km away, the waves had an inundation height of about 1.5 m, but they persisted for such a long time that they caused damage to the harbor works and loss of life around Keti Bandar on the coast of the Indus delta. Based on Ambraseys and Melville's (1982) report, tsunami waves reached heights of up to 2 m, causing some loss of life in the region of Bombay, more than 1100 km away from Pasni. Similarly, Pendse (1946) and

Berninghausen (1966) have also estimated about 1.5 and 2 m for the wave heights at Karachi and Bombay, respectively.

The 1945 tsunami waves were also observed at the southwest coasts of Iran, though there is no specific information about their run-up heights, and no casualties were reported due to the general low population of the area and the high topography of the few populated locations. Recently, Hamzeh et al. (2013) and Okal et al. (2015) estimated the tsunami wave heights at different parts of the Iranian coast, from Pozm Bay to Pasabadanr at the west corner of Gwadar Bay on the maritime border of Pakistan and Iran, using field surveys and interviews with local elderly people who remembered the event. According to their study, the 1945 tsunami waves had heights of about 8, 5 and 2 m at Pasabandar, Beris and Chabahar ports, respectively. Figure 2 shows a summary of the reported wave heights of 1945 Makran tsunami along the coasts of Pakistan and Iran according to different researchers.

Assuming the 1945 earthquake as the source, the Makran tsunami has been numerically simulated by many researchers (e.g., Heidarzadeh et al. 2009; Rajendran et al. 2008; Neetu et al. 2011). However, the simulated tsunami waves at the various coastlines do not agree with the existing reports and field data. Disagreements exist regarding both the wave heights and arrival times. For example, numerical simulations result in a tsunami wave height of 4–5 m at Pasni (Heidarzadeh et al. 2009; Rajendran et al. 2008), which is much lower than the values mentioned above. Another major difference is the significant delay in arrival of tsunami waves with respect to the time of the quake shakings. Based on the modeling results, the first tsunami wave hits the coasts of Makran about 1 h after the quake (Heidarzadeh et al. 2009; Rajendran et al. 2008). However, available data reveal that the second and third tsunami high waves attacked the coasts a few hours after the shock (Ambraseys and Melville 1982; Pendse 1948).

Neetu et al. (2011) also modeled the 1945 Makran tsunami and demonstrated the persistent high waves due to trapping of the tsunami wave energy on the continental shelf off the Makran coasts to overcome the discrepancy mentioned previously. They concluded that the persistence of high waves is the reason of the reported time lag between the first and second tsunami waves. However, although their simulation does show second and third waves, the modeled wave heights at coasts of Pasni and Omara were in the order of 2 m,

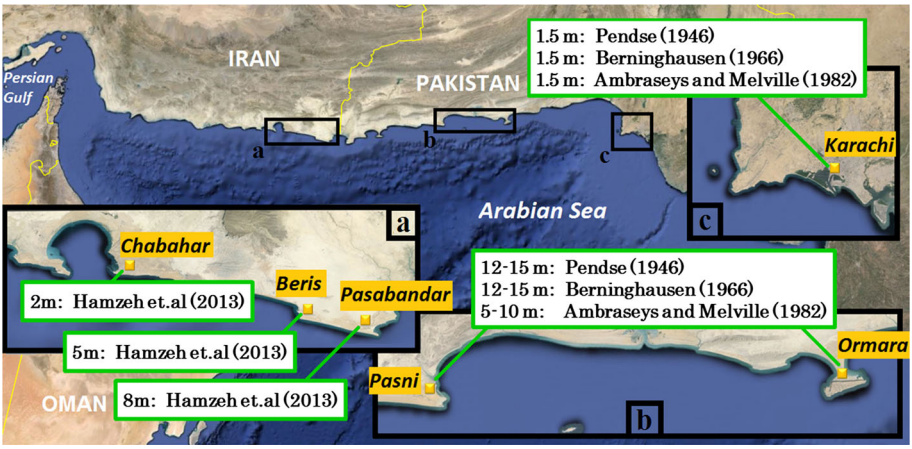

Fig. 2 Reported wave heights of the 1945 Makran tsunami along the coasts of Pakistan and Iran

i.e., far below the reported run-up values, which cannot be responsible for the fatalities and vast damages that were recorded at these two cities.

The above disparity in modeling results between the different studies and reported tsunami surges can be attributed to a secondary non-seismic tsunami, such as a submarine landslide, triggered by earthquake. Although this scenario has been mentioned by some other researchers (e.g., Rajendran et al. 2008; Neetu et al. 2011), such a simulation was not conducted mainly due to absence of the required information about the characteristics of the probable landslide and also limited measurements of tsunami heights along neighboring coasts.

3 Simulation of 1945 Makran seismic tsunami

The propagation of tsunamis due to earthquakes is commonly described by shallow water equations, i.e., the simplest form of depth integrated long wave equations, since their wavelengths, in the order of hundreds of kilometers, are much larger than the ocean depth, in the order of few kilometers. The MOST numerical model (Titov and Gonzales 1997), developed based on 2D Nonlinear Shallow Water (NSW) equations, is applied here to model the 1945 Makran tsunami caused by the movement of tectonic plates. As the calculation of the inundation stage requires higher resolution topography and hydrography

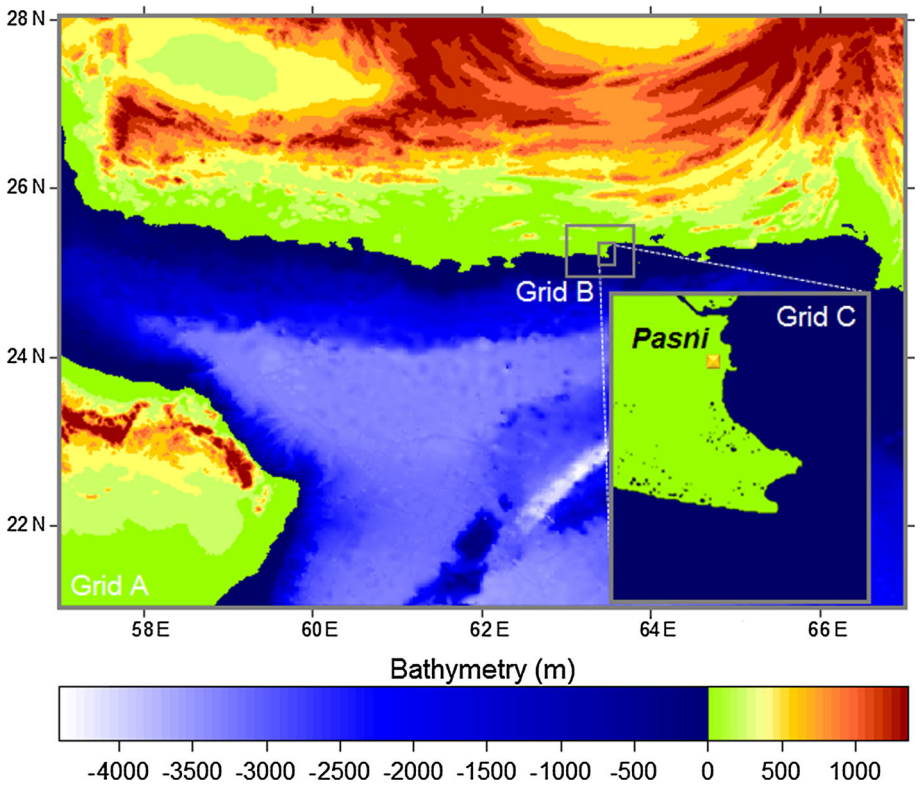

Fig. 3 Nested grid of model domain

data, in comparison with the propagation stage of tsunami, the NSW equations are solved in a three-level nested grid model domain, where the grid resolution increases when moving from deep water toward the nearshore coastal areas.

Figure 3 shows three grids (A, B and C) of the computational model domain. The first one (grid A) covers all of the MSZ between 57–67°E and 21–28°N at a resolution of 1 arcmin (about 1800 m); and the third one (grid C) is localized at Pasni between 63.43–63.53°E and 25.11–25.23°N at a resolution of 3 arcsec (about 90 m). The topography data of grid C were extracted from a high-resolution digital topographic database of the Earth generated by Shuttle Radar Topography Mission (SRTM), while its hydrographic data were obtained from global 30 arcsec grid of General Bathymetric Chart of the Oceans (GEBCO) and they were integrated with topography data using interpolation.

Employing the elastic deformation model of Okada (1985), the source parameters of 1945 earthquake estimated by Byrne et al. (1992) are introduced to the MOST model to calculate seabed vertical displacements (Table 1). As earthquake tsunamis are generated instantaneously, seabed displacements are simultaneously transferred to initial sea surface elevations. Introducing the calculated free surface elevations to the numerical model as an initial condition, the propagation of 1945 tsunami was simulated by solving the NSW equations all over the computational domain.

In order to obtain the tsunami wave heights, time series of the tsunami waves were extracted at some numerical stations of grid C in the vicinity of Pasni (Fig. 4). Figure 5 shows the time series at numerical stations, presenting wave heights of about 4.5 and 1 m at the outer (O, P and Q) and inner (R, S and T) stations along the coasts, respectively. The wave heights considerably decrease at the inner coasts as they are protected from direct attack of tsunami waves. The discontinuity of the lines at some stations is due to drying of the coast when water level recedes.

As large-scale grids were employed in past simulations of 1945 Makran tsunami, other researchers could not accurately define the tsunami wave heights along the coastline and the outputs of their numerical models at Pasni should be compared with our tsunami waves at outer coasts of grid C. The simulated wave heights of about 4–5 m at the outer coasts (stations O, P and Q) are therefore in agreement with the numerical results of Rajendran et al. (2008) and Heidarzadeh et al. (2009) at Pasni. Water levels at other areas also agree with published numerical results by other authors. For example, the model results in a tsunami wave height of <1 m along the entire Iranian coastline (Heidarzadeh et al. 2009). However, the comparison between the model outputs and actual reported tsunami wave heights (Fig. 2) reveals a large disparity. Considering that using a fine grid in the present simulation resulted in a lower simulated tsunami wave height at Pasni, in the order of 1 m in comparison with previous simulated results of about 4–5 m, the gap between the modeling output and reported observation at Pasni can be considered to be wider. Moreover, the modeled tsunami wave heights along the coasts of Iran are similarly much lower than the recent field data of Hamzeh et al. (2013) and Okal et al. (2015).

Table 1 Estimated parameters of the 1945 Earthquake (Byrne et al. 1992)

Earthquake epicenter	Fault length (km)	Fault width (km)	Fault depth (km)	Fault slip (m)	Dip angle (°)	Strike angle (°)	Rake angle (°)
25.15°N 63.48°E	150	100	27	7	7	246	89

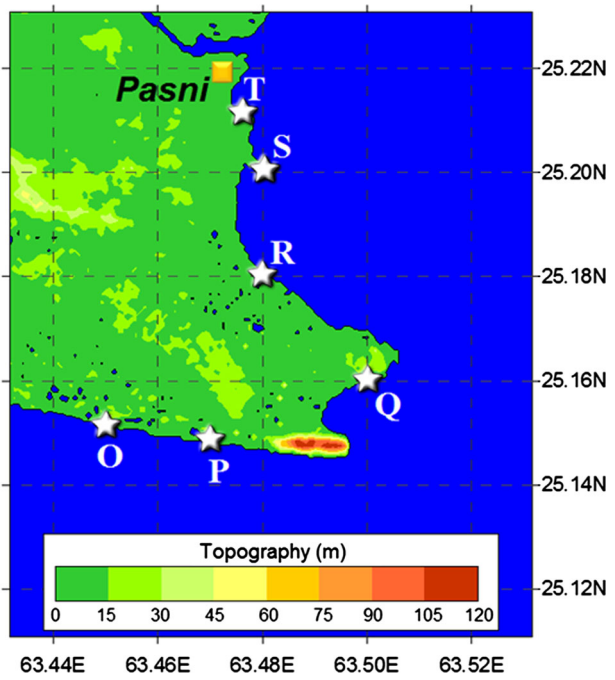

Fig. 4 Numerical wave stations and topography of grid C

The facts presented above indicate that a non-seismic source, such as a submarine landslide, could have been the primary cause of 1945 Makran tsunami. The delay in arrival time of the tsunami waves can also be attributed to the time taken for slumping along the continental slope (Rajendran et al. 2008). Moreover, extensive cutting of the transoceanic cables between India and Britain and the slide of coastal part of the Pasni beneath the sea are two important observed records after the 1945 quake that support the large-scale ground motion. Byrne et al. (1992) also reported that the coastal part of the town of Pasni slipped south beneath the sea, with one of the submarine slides also showing intense liquefaction, both indicating large-scale ground motion. These evidences highly increase the probability that a huge submarine landslide could have taken place following 1945 earthquake (Ambraseys and Melville 1982).

The potential for tsunami triggering by slides has been already observed in different events, including the 1958 Lituya Bay, South East Alaska earthquake, which triggered a subaerial landslide that caused a severe impact to the coast (Miller 1960) and the 1998 Papua New Guinea, which caused a destructive tsunami with waves up to 15 m high and about 2200 fatalities (McSaveney et al. 2000).

4 Simulation of 1945 Makran tsunami caused by a submarine landslide

The new scenario of the 1945 tsunami that considers a probable submarine landslide triggered by the earthquake was simulated using the GEOWAVE model. GEOWAVE, a combination of TOPICS and FUNWAVE models, is an integrated tsunami simulation

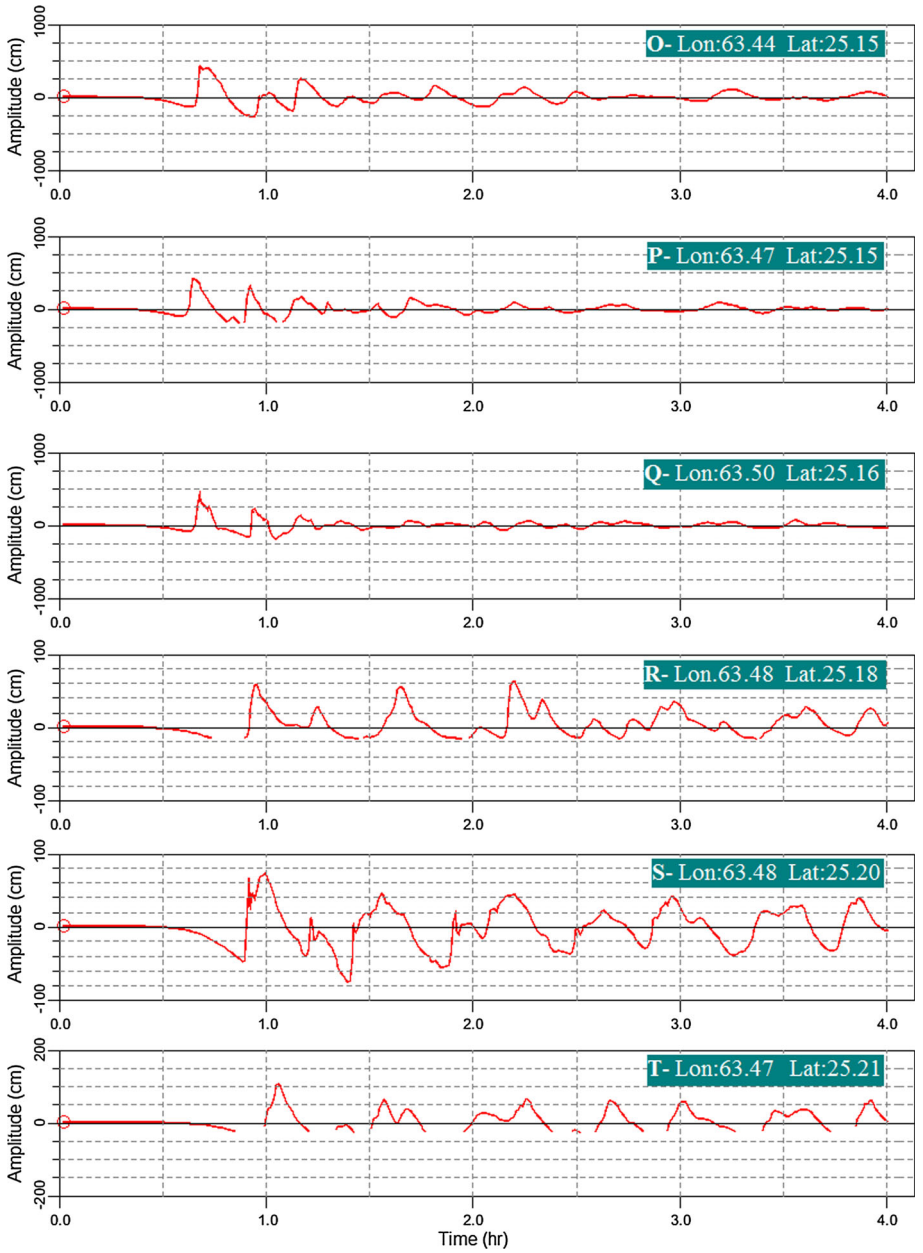

Fig. 5 Wave height time series of the numerical wave stations of grid C

numerical model where the first stage of modeling, i.e., tsunami generation, and later stages, i.e., propagation and inundation, are simulated by TOPICS and FUNWAVE, respectively.

TOPICS, the tsunami generator model of GEOWAVE, can simulate multiple tsunami sources with different mechanisms of generation. In order to calculate the initial free surface elevation due to submarine landslides, the model uses predictive equations of characteristic wavelength and wave amplitude, developed by Grilli and Watts (2005) based on the results of 2D fully nonlinear potential flow model.

Two idealized types of submarine mass failures moving over plane slopes are considered in this model, representing the extreme cases of a general probable submarine mass failure motion. These two types are underwater slides, i.e., translational failures, and slumps, i.e., rotational failures. For underwater slides, which is the probable scenario for the Makran submarine landslide, the landslide is idealized as a mound with elliptical cross section translating along a straight slope θ (Fig. 6). The mound is specified with maximum thickness T in the middle, total length b along the down-slope axis, total width w along the cross-slope axis, and an initial submergence d at the middle of the landslide. According to the presented predictive equations, the initial tsunami wave depends on the volume of the sliding body (b, w, T), initial submergence and seabed slope, which are not known for the case of this hypothesized Makran submarine landslide. Thus, the authors attempted to determine them using a trial and error approach, considering the reported wave heights at different regions.

Landslides tsunamis have high local effect and limited far-field effect, because of their radial damping and frequency dispersion (Masson et al. 2006). As the maximum heights of the 1945 tsunami waves were reported at Pasni and Ormara, the location of probable submarine landslide is thus assumed to be located somewhere between these two ports. Thus, the seabed slope and initial submergence of slide are estimated according to this landslide location. On the other hand, and given the high waves of the 1945 tsunami and proportional relation between wave height and sliding body volume, the probable landslide is assumed to be massive and the parameters (b, w, T) defining the volume are estimated according to normal dimensions of observed submarine landslides (Table 2). By feeding the properties of the hypothesized Makran submarine landslide to TOPICS, the initial tsunami wave (initial sea surface elevation) is finally calculated and applied to the model (Fig. 7) The modeling domain covers the MSZ between Chabahar Bay and Karachi at a resolution of 30 arcsec.

As landslide tsunami waves are shorter in comparison with those generated by earthquake tsunamis, the effect of frequency dispersion is higher and they cannot be accurately simulated by shallow water equations, which disregard frequency dispersion. Moreover,

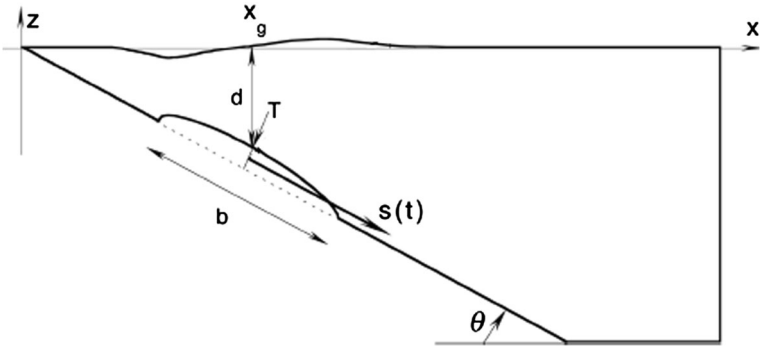

Fig. 6 Definition sketch of the simulation domain for underwater slides (Grilli and Watts 2005)

Table 2 Parameters of the probable 1945 submarine landslide

Landslide center	Initial submergence (m)	Seabed slope (°)	Slide length (Km)	Slide thickness (Km)	Slide width (Km)
24.75°N 64.10°E	1134	6	15	0.5	10

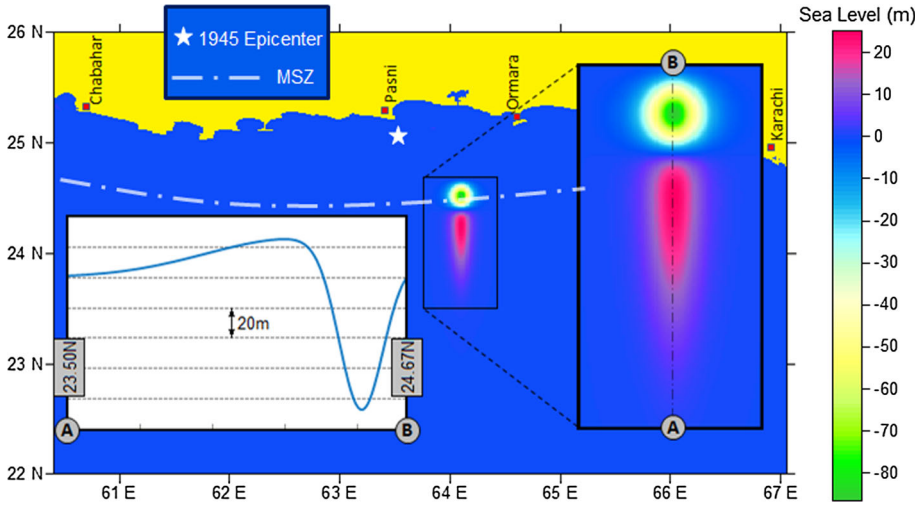

Fig. 7 Initial free surface elevation caused by probable 1945 submarine landslide

these tsunami waves are non-hydrostatic. Hence, a different approach is necessary for their numerical modeling. GEOWAVE simulates tsunami propagation and inundation using the long wave propagation model FUNWAVE (Kennedy et al. 2000; Chen et al. 2000) based on fully nonlinear Boussinesq equations developed by Wei et al. (1995), considering the effects of nonlinearity and frequency dispersion. These equations, expressing conservation of mass and momentum, are respectively, given by:

$$\eta_t + \nabla \cdot \left\{ (h+\eta) \left[u_\alpha + \left(z_\alpha + \frac{1}{2}(h-\eta) \right) \nabla(\nabla \cdot (h u_\alpha)) + \left(\frac{1}{2} z_\alpha^2 - \frac{1}{6}\left(h^2 - h\eta + \eta^2\right) \right) \nabla(\nabla \cdot u_\alpha) \right] \right\} = 0$$

$$u_{\alpha t} + (u_\alpha \cdot \nabla) u_\alpha + g\nabla\eta + z_\alpha \left\{ \frac{1}{2} z_\alpha \nabla(\nabla \cdot u_{\alpha t}) + \nabla(\nabla \cdot (h u_{\alpha t})) \right\} + \nabla \left\{ \frac{1}{2}\left(z_\alpha^2 - \eta^2\right)(u_\varepsilon \cdot \nabla)(\nabla \cdot u_\alpha) + \frac{1}{2}[\nabla \cdot (h u_\alpha) + \eta \nabla \cdot u_\alpha]^2 \right\} + \nabla \left\{ (z_\alpha - \eta)(u_\varepsilon \cdot \nabla)(\nabla \cdot (h u_\alpha)) - \eta \left[\frac{1}{2}\eta \nabla \cdot u_{\alpha t} + \nabla \cdot (h u_{\alpha t}) \right] \right\} = 0$$

where η is the surface elevation, h is still water depth, u_α is the horizontal velocity vector at water depth $z = z_\alpha = -0.531\ h$, $\nabla = (\partial/\partial x, \partial/\partial y)$ is the horizontal gradient operator and

subscript t is the partial derivative with respect to time. The initial free surface elevation, calculated by TOPICS, provides the initial condition for the governing equations. Using the finite difference technique and a composite fourth-order Adams–Bashforth–Moultan scheme, the equations are solved in model domain and the surface elevation and velocities are calculated in any time step of the simulation. Considering the mesh size, i.e., 30 arcsec (about 900 m), a time step of $dt = 1.22$ s was determined by the model to satisfy the stability conditions. Figure 8 displays the propagating tsunami waves, computed by the FUNWAVE model. It is observed that tsunami waves propagate out from the landslide location in circular rings. The waves highly damp at first, when they leave the landslide location; but they amplify approaching the coast of neighboring countries, because of shoaling. The waves also persist for a long time at the vicinity of the coasts. In order to have a better view of the waveforms at different locations, point stations were defined along the Makran coastline. Figure 9 shows the location of the numerical stations used, and the recorded time series of tsunami waves are presented in Fig. 10.

The time series of the wave heights at stations D, E, F and G in Fig. 10 reveal that falling water is first observed along the coastlines of Pakistan. As the landslide movement is toward the south direction (because of the bathymetry of the region), the trough of the tsunami wave is created behind the landslide (See Fig. 7). It can also be observed that the neighboring coasts are strongly affected and highly flooded by this landslide tsunami, as expected. The maximum wave height at Pasni (station D) is about 8 m, while tsunami waves at the west and east coasts of Ormara (stations E and F) are about 11 and 7 m high, respectively. The results at other numerical stations located long distances away from the landslide location, such as Karachi and cities in south of Iran, show much lower tsunami waves, which was expected due to the limited far-field effect of landslide tsunamis. The differences of tsunami wave heights between the coasts located close and far to the landslide can also be observed in Fig. 11, which depicts the maximum wave heights along the coastal areas of Pakistan and Iran.

5 Discussion

Assuming the occurrence of a major landslide, Table 3 shows the comparisons between the simulated and reported tsunami wave heights at selected locations. Unlike the previous simulations, based on a seismic tsunami, an acceptable agreement between simulated and observed values is observed all over the Makran coastline. Also, it is now possible to explain the reported time lag between the arrival of tsunami high waves and the earthquake shock using the time series of Fig. 10.

Based on Pendse's (1948) report, the second wave of the tsunami (far more damaging than the first one) reached to the coasts of Pasni at about 7:15 a.m. local time, a few hours after arrival of small first wave. It should be mentioned that Ambraseys and Melville (1982) reported the second and third waves of tsunami were observed at Pasni at about 5:00 a.m.; but the timings reported by Pendse (1948) are followed here, because of their agreement with the Survey of the Indian data (Rajendran et al. 2008). Tsunami waves were also observed at the shores of Karachi 5 h after the quake shock (The Times of India, Poona, November 29, 1945), i.e., about 8:00 a.m. local time.

Despite the valuable historical reports providing tsunami details for the coasts of Pakistan and India, there is unfortunately no valid historical document that provides any characteristics of the tsunami waves along Iranian coasts. The only available information

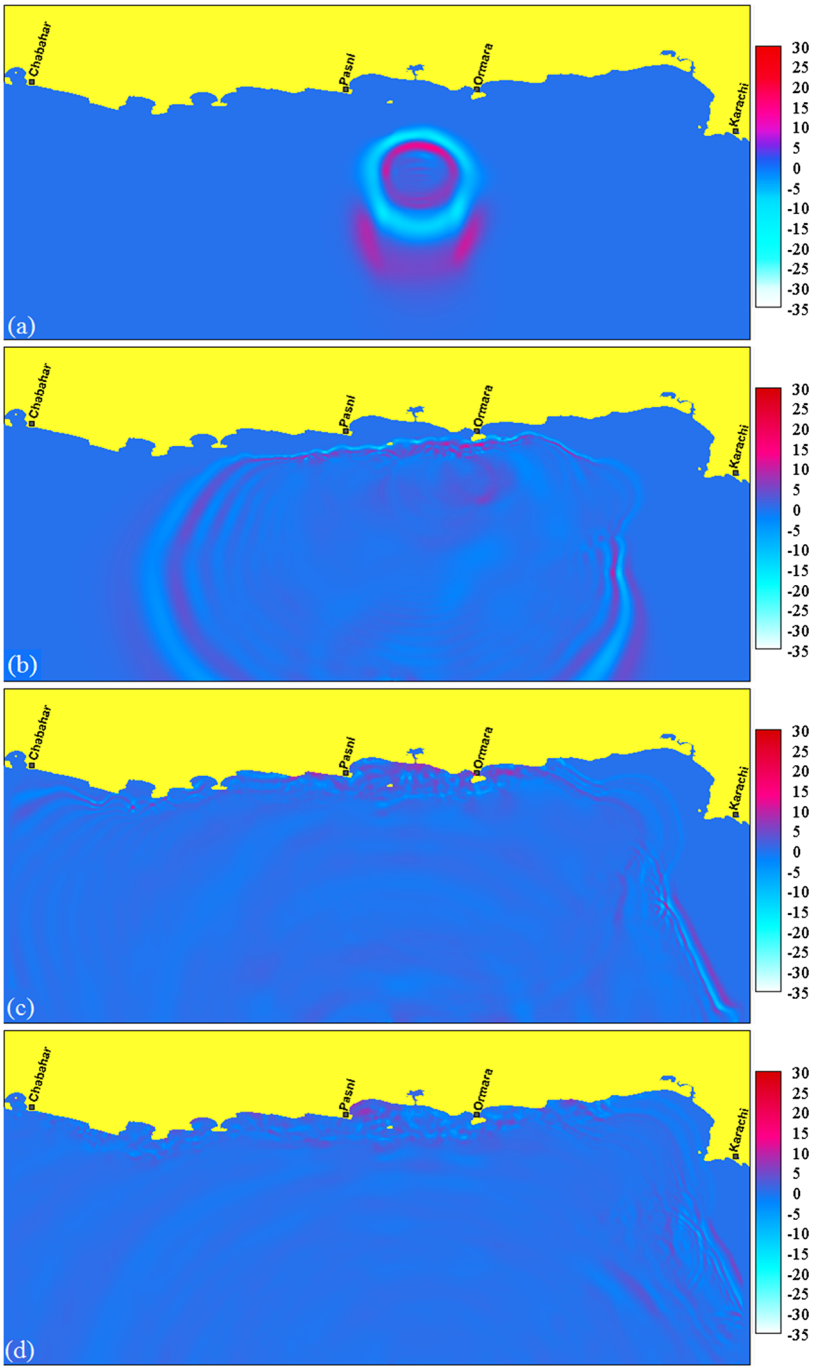

Fig. 8 Computed tsunami waves in meters propagating at **a** 5, **b** 25, **c** 45 and **d** 65 min after the generation of initial wave

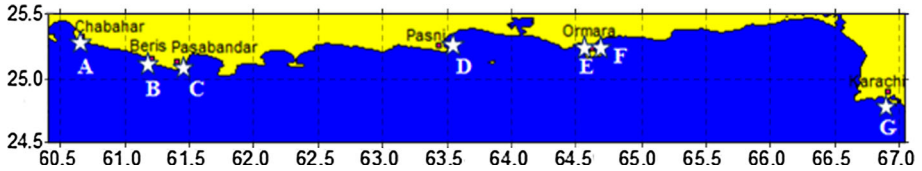

Fig. 9 Location of numerical wave stations (*A*–*G*)

was recently obtained through field surveys and interviews with the elderly people of Chabahar Bay (Hamzeh et al. 2013; UNESCO/IOC 2015). Although the reported water levels by field surveys look reasonable, many inconsistencies exist regarding the arrival times of tsunami waves, which can be expected to some extent given the long time that has passed since 1945 Tsunami. As an example, one interviewer mentioned that "three huge waves struck the Konarak around 8 a.m., Iran time" (UNESCO/IOC 2015), while another declared that the arrival time of tsunami waves to Konarak was around morning prayer time (Hamzeh et al. 2013; UNESCO/IOC 2015), which is about 4:30 a.m. Iran time at the end of November for Konarak. There are similar contradictions in the declared arrival times of tsunami waves to Chabahar and Ramin. Based on the statements of interviewers, tsunami waves attacked the coasts of Chabahar and Ramin at about 3:30 a.m. and after 8:00 a.m., respectively (UNESCO/IOC 2015). However, such a large difference of arrival times is not logical, considering that the distance between these two cities is only about 10 km. Moreover, and contrary to the descriptions of interviewees, it would be expected that tsunami waves arrive to Ramin before Chabahar, as Ramin is located to the east of Chabahar, i.e., closer to the tsunami source. Because of the above contradictions in the interviews conducted, it is does not seem to be possible to accurately judge the arrival times of tsunami waves to Iranian coastlines due to this earthquake.

According to the simulated time series, tsunami waves would have come to the coasts of Pasni and Ormara about 40 min after the occurrence of the probable submarine landslide (stations D and E); and they were observed at the coasts of Karachi about 115 min after the landslide (stations G). Thus, if the occurrence time of the probable submarine landslide is assumed to be about 3.5 h after the earthquake (at around 6:30 a.m.), the calculated arrival times of tsunami waves at different regions of Makran coasts would be in agreement with reported observations, as presented in Table 4. It is important to note that Table 4 shows the reported arrival time of the second wave to Pasni. The first small wave, probably generated by earthquake, reached the coast of Pasni in about half an hour, but a greater damage was caused by the second wave (Pendse 1948; Ambraseys and Melville 1982). However, Table 4 presents the arrival time of the submarine wave to Karachi because seismic tsunami waves did not affect this area.

It should be noted that the time and the characteristics of the probable submarine landslide have been hypothetically determined in the above modeling. Although the assumed 3.5 h lag between the earthquake and the triggered landslide seems to be unusually large, in comparison with past reported landslides in the world, it is possible that a landslide follows an earthquake few tens of minutes later, according to complex nucleation of a failure plane, or to a mild secondary aftershock (Synolakis et al. 2002). As an example, 2-h delay was reported between the times of the earthquake and the following landslide in 1990 Rudbar at the south coast of Caspian Sea, which was attributed to the nonlinearity of the triggering process, probably involving an evolution of fluid pore pressure inside the rock (Salaree and Okal 2015). On the other hand, there are some

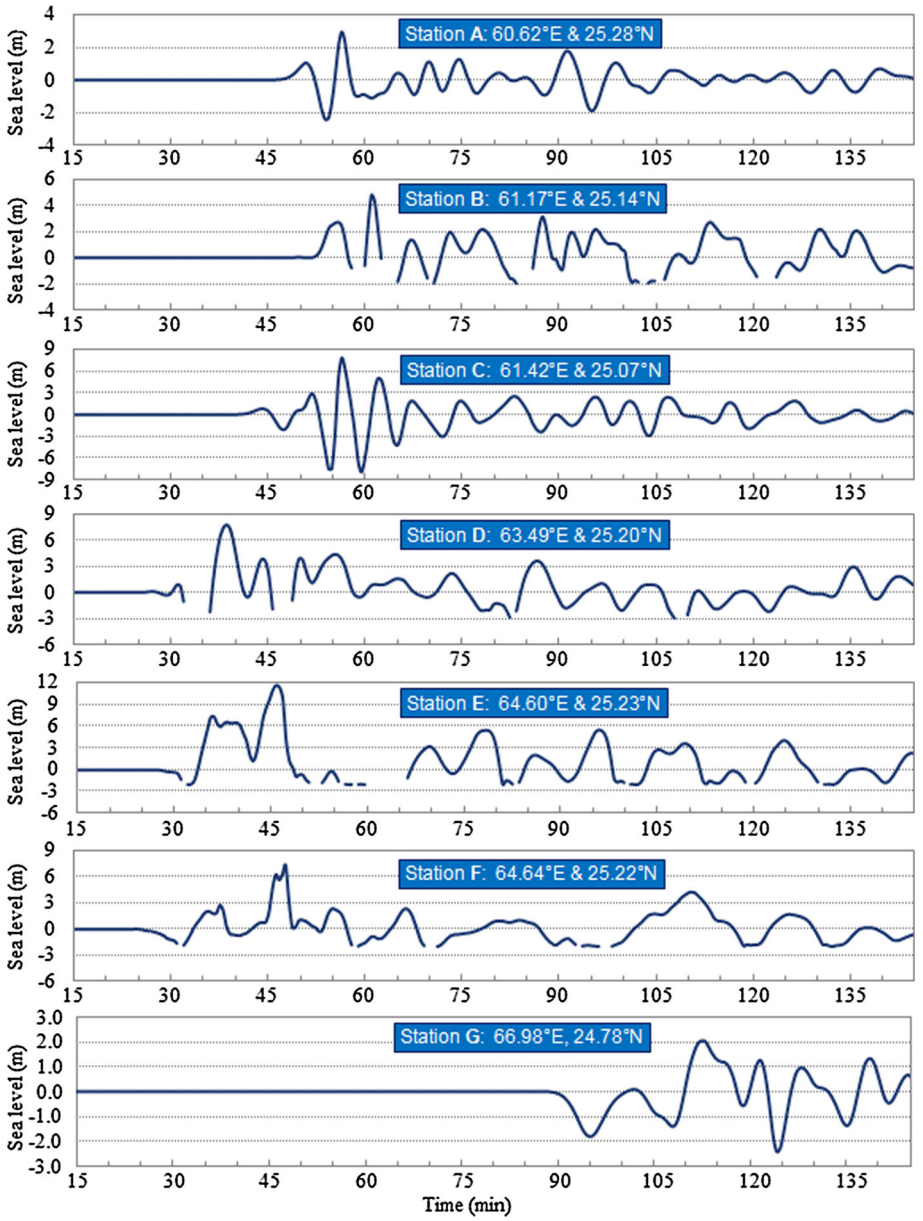

Fig. 10 Wave height time series for numerical wave stations

inevitable errors in the information available and observations of 1945 tsunami that cannot be clearly defined. Thus, full agreement between simulation results and existing reports are unlikely to ever be achieved. Nevertheless, unlike previous modeling studies, the assumption of a submarine landslide as a second tsunami generating mechanism after initial (small one) generated by the 1945 earthquake resolves the discrepancies between the simulated results and reported observations. Besides acceptable outputs of tsunami wave

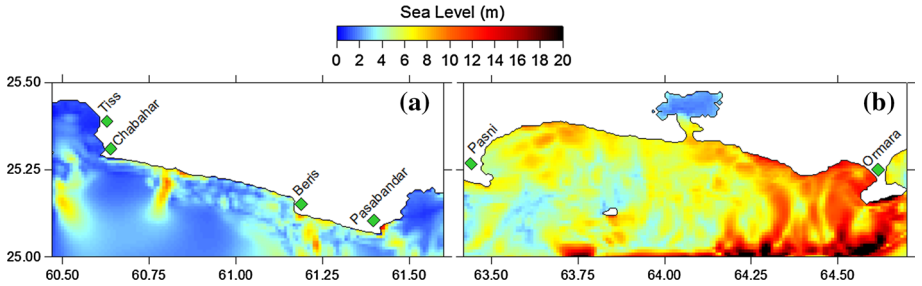

Fig. 11 Maximum calculated tsunami wave heights along some coastal areas of **a** Iran and **b** Pakistan

Table 3 Comparisons between simulated and reported heights of 1945 tsunami waves

Location	Simulated wave height (m)	Reported wave height (m)
Chabahar	2.98	2[a], 2.76[b]
Beris	4.79	5[a], 5.02[b]
Pasabandar	7.81	8[a], 9.71[b]
Pasni	7.73	5–10[c], 12–15[d, e]
Ormara	11.58	5–10[c], 12–15[d, e]
Karachi	2.05	1.5[c, d, e]

[a] Hamzeh et al.(2013)

[b] Okal et al. (2015) (Run-up)

[c] Ambraseys and Melville (1982)

[d] Berninghausen (1966)

[e] Pendse (1946)

Table 4 Comparisons between simulated and reported arrival times of 1945 tsunami waves

Location	Simulated travel time[a] (min)	Simulated arrival time[b] (h:m)	Reported arrival time (h:m)
Pasni	38	7:08	7:15[c]
Karachi	112	8:22	8:00[d]

[a] Time distance between landslide and waves arrival (according to Fig. 10 time series)

[b] Assumed time of probable landslide (6:30 a.m.) plus travel time

[c] Pendse (1948)

[d] Times of India, Poona, November 29, 1945

heights and arrival times of 1945 Makran tsunami in this new scenario, the persistency of the tsunami waves along Makran coasts, reported in earlier studies of Ambraseys and Melville (1982) and Neetu et al. (2011), is also observed in the oscillations of the calculated time series of Fig. 10. It can be concluded that the new hypothesis of considering a non-seismic submarine landslide as the major source of 1945 Makran tsunami is able to accurately reproduce the tsunami characteristics in neighboring countries and successfully overcomes the disagreements between the observations and past modeling results.

6 Summary and conclusions

Previous simulations of the 1945 Makran tsunami have shown a lack of agreement with the data of existing reports at many locations, regarding both tsunami wave heights and arrival times. To overcome this discrepancy, the present study presents a hypothesis that considers a submarine landslide as the major source of 1945 Makran tsunami, and proceeds to simulate the likely characteristics of such an event.

In order to highlight the nature of the discrepancies between the classic earthquake source scenario and historical observations, the 1945 tsunami was first simulated based on the assumptions regarding the seismic source, using the MOST model. A fine nested grid was applied near the coasts in order to increase the accuracy of model outputs. However, mismatches between the reported tsunami waves and simulated values were still observed. Then, the authors proceeded to model the hypothesis of a 1945 Makran tsunami caused by a probable submarine landslide, where the GEOWAVE model, a combination of TOPICS and FUNWAVE models, was applied. The initial tsunami wave was calculated by TOPICS using several assumptions regarding the location and dimensions of the slide, and the propagation and inundation of the tsunami was simulated by FUNWAVE, based on fully nonlinear Boussinesq equations considering the effects of nonlinearity and frequency dispersion.

The simulated landslide tsunami showed good results in comparisons with reported wave heights at different coasts. The calculated arrival times of tsunami waves at different regions of Makran coasts can also be explained well if the occurrence time of submarine landslide is assumed to be about 3.5 h after the earthquake, at around 6:30 a.m. (local time).

It should be added that because of the lack of small-scale bathymetry data, it was not possible to accurately estimate the location and dimensions of the presumed landslide in the preliminary modeling of this study. As signatures of massive landslides are well preserved in the oceans, future geological or bathymetric surveys are necessary for a refined numerical modeling of landslide tsunami.

A submarine slide tsunami in the thick unconsolidated sediments of the MSZ (Bourget et al. 2011) is an underestimated potential threat in the Arabian Sea and Gulf of Oman. Further studies on the possibility of the occurrence of submarine landslides in the region, such as investigating the structure of the uppermost sediments of the Gulf of Oman, are necessary for the assessment of tsunami hazards in MSZ. It is crucial that the regional tsunami hazard models combine such overlooked mechanism with seismic tsunamis in the development and implementation of a tsunami warning system, which is necessary from the point of view of public safety, and the development of other countermeasures to reduce the damages to coastal properties and infrastructure.

References

Ambraseys NN, Melville CP (1982) A history of Persian earthquakes. Cambridge University Press, Britain

Berninghausen WH (1966) Tsunamis and seismic seiches reported from regions adjacent to the Indian Ocean. Bull Seismol Soc Am 56(1):69–74

Bourget J, Zaragosi S, Ellouz-zimmermann N, Mouchot N, Garlan T, Schneider J, Lanfumay V, Lallemant S (2011) Turbidite system architecture and sedimentary processes along topographically complex slopes: the Makran convergent margin. Sedimentology 58:376–406

Byrne DE, Sykes LR, Davis DM (1992) Great thrust earthquakes and aseismic slip along the plate boundary of the Makran subduction zone. J Geophys Res 97:449–478
Chen Q, Kirby JT, Dalrymple RA, Kennedy AB, Chawla A (2000) Boussinesq modelling of wave transformation, breaking, and runup; II: 2D. J Waterw Port Coast Ocean Eng 126(1):48–56
Grilli ST, Watts P (2005) Tsunami generation by submarine mass failure; I: modeling, experimental validation, and sensitivity analyses. J Waterw Port Coast Ocean Eng 131:283–297
Hamzeh MA, Okal EA, Ghasemzadeh J, Baskaleh GR (2013) Investigation of 1945 Pakistan tsunami's effect on Iranian coasts of Makran. National Conference on Makran Coasts Development and Maritime Authority of Islamic Republic of Iran, Paper number 1123 **(in Persian)**
Heck NH (1947) List of seismic sea waves. Bull Seismol Soc Am 37(4):269–286
Heidarzadeh M, Pirooz MD, Zaker NH, Yalciner AC, Mokhtari M, Esmaeily A (2008) Historical tsunami in the Makran subduction zone off the southern coasts of Iran and Pakistan and results of numerical modeling. Ocean Eng 35(8&9):774–786
Heidarzadeh M, Pirooz MD, Zaker NH, Yalciner AC (2009) Preliminary estimation of the tsunami hazards associated with the Makran subduction zone at the northwestern Indian Ocean. Nat Hazards 48(2):229–243
Kennedy AB, Chen Q, Kirby JT, Dalrymple RA (2000) Boussinesq modeling of wave transformation, breaking, and runup; I: 1D. J Waterw Port Coast Ocean Eng 126(1):39–47
Lisitzin E (1974) Sea level changes. Elsevier, New York, p 273
Masson DG, Harbitz CB, Wynn RB, Goldsmith P, Pedersen G, Lovholt F (2006) Submarine landslides: processes, triggers, and hazard prediction. Philos Trans R Soc A 364:2009–2039
McSaveney MJ, Goff JR, Darby DJ, Goldsmith P, Barnett A, Elliot S, Nongkas M (2000) The 17 July 1998 tsunami, Papua New Guinea: evidence and initial interpretation. Mar Geol 170:81–89
Miller DJ (1960) The Alaska earthquake of 10 July 1958: giant wave in Lituya Bay. Bull Seismol Soc Am 50:253–266
Murty TS, Bapat A (1999) Tsunamis on the Coastlines of India. Sci Tsunami Hazards 17(3):167–172
Neetu S, Suresh I, Shankar R, Nagarajan B, Sharma R, Shenoi SSC, Unnikrishnan AS, Sundar D (2011) Trapped waves of the 27 November 1945 Makran tsunami: observations and numerical modeling. Nat Hazards 59(3):1609–1618
Okada Y (1985) Surface deformation due to shear and tensile faults in a half-space. Bull Seismol Soc Am 75(4):1135–1154
Okal EA, Fritz HM, Hamzeh MA, Ghasemzadeh J (2015) Field survey of the 1945 Makran and 2004 Indian Ocean tsunamis in Baluchistan, Iran. Pure appl Geophys. doi:10.1007/s00024-015-1157-z
Pendse CG (1946) The Mekran earthquake of the 28th November 1945. India Meteorol Depart Sci Notes 10(125):141–145
Pendse CG (1948) A short note on the Mekran earthquake of the 28 November 1945. J Sci Ind Res 5:106–108
Rajendran CP, Ramanamurthy MV, Reddy NT, Rajendran K (2008) Hazard implications of the late arrival of the 1945 Makran tsunami. Curr Sci 95:1739–1743
Salaree A, Okal EA (2015) Field survey and modeling of the Caspian Sea tsunami of 20 June 1990. Geophys J Int 201:621–639
Smith GL, McNeill LC, Wang K, He J, Henstock TJ (2013) Thermal structure and megathrust seismogenic potential of the Makran subduction zone. Geophys Res Lett. doi:10.1002/grl.50374
Synolakis CE, Bardet JP, Borrero JC, Davies HL, Okal EA, Silver EA, Sweet J, Tappin DR (2002) Slump origin of the 1998 Papua New Guinea tsunami. Proc Roy Soc (Lond) Ser A 458:763–789
Titov VV, Gonzales FI (1997) Implementation and testing of the method of splitting tsunami (MOST) model. NOAA Technical Memorandum ERL-PMEL-112, PB98-122773, Pacific Marine Environmental Laboratory, Seattle, p 11
UNESCO/IOC (2009) Tsunami risk assessment and mitigation for the Indian Ocean; knowing your tsunami risk—and what to do about it. IOC Manual and Guides 52, Paris
UNESCO/IOC (2015) Remembering the 1945 Makran Tsunami; Interviews with Survivors Beside the Arabian Sea. IOC Brochure 2015-1, Paris
Wei G, Kirby JT, Grilli ST, Subramanya R (1995) Fully nonlinear Boussinesq model for free surface waves; Part 1: highly nonlinear unsteady waves. J Fluid Mech 294:71–92